Effect of Feed-Stream Configuration on Gas-Phase Chlorination Reactor Performance

Venkatramanan Raman* and Rodney O. Fox

Department of Chemical Engineering, Iowa State University, Ames, Iowa 50011-2230

Albert D. Harvey III and David H. West

The Dow Chemical Company, Freeport, Texas 77541-3257

Chlorination of hydrocarbons is an industrially important process used for the production of commercially viable environmentally friendly chemicals. The highly exothermic nature of these reactions necessitates a thorough study of reactor stability and product feasibility. Here, computational fluid dynamics (CFD) is used to analyze the performance of a coaxial right-cylindrical insulated reactor for different inlet flow configurations. Chlorination reactions involve a large number of radicals and other intermediates, and hence, direct simulations using traditional CFD techniques are difficult because of the stiff nature of the reaction scheme involved. A novel algorithm for reaction computation, in situ adaptive tabulation (ISAT), is used to obtain considerable computational gains. The joint probability density function (JPDF) transport equation for the scalars with closed terms for reaction is solved using a Monte Carlo particle algorithm in tandem with a finite-volume (FV) Reynolds-averaged Navier−Stokes (RANS) method. The particle method handles transport of 15 scalars along with enthalpy and feeds back mean field values of temperature and molecular weight that are used by the FV code to correct the flow for reaction. The scalar scatter plots conditioned on the mixture fraction are used to study the details of the kinetics in different reactor zones. Comparison of premixed and segregated inlets is done to determine reactor stability and product yield. Conclusions are then drawn about fundamental properties of the reactor and broad considerations for reactor design.

I. Introduction

Chlorinated hydrocarbons are an important class of industrial chemicals. Chloroform, carbon tetrachloride, allyl chloride, benzyl chloride, and trichloroethene are some of the common products that belong to this group. Chlorinated hydrocarbons are used in aerosol product formulation, chemical processing, dry cleaning, metal cleaning/degreasing, paint formulation, and pharmaceuticals manufacturing. High-temperature gas-phase chlorination is an economically viable process for the production of these chemicals. The process studied here is used to produce chloroform from a mixture of methyl chloride and methyl dichloride that is mixed with pure chlorine. The product mixture also contains carbon tetrachloride (which is the competing product) and hydrogen chloride (produced as a byproduct in secondary and tertiary chlorination). The methyl dichloride fraction remains almost unchanged and is separated from the product mixture before being fed back to the reactor. Despite the simplicity of the chlorination operation, control over the product distribution is difficult and essential in obtaining good chloroform yields. Chlorination of methyl chloride proceeds by a free-radical mechanism involving chlorine atoms and organic free radicals as chain carriers. The first process is the disassociation of the chlorine molecule. The introduction of a single chlorine atom or an organic free radical can result in chain-propagating reactions. The overall rate depends on the competition between chain-initiating and chain-terminating reactions. It is known that the maximum yield of chloroform and other secondary chlorinated products occurs at 700−740 K for the reactant mixture used here. Higher temperatures lead to product decomposition and formation of double- and triple-bonded hydrocarbons. At the same time, longer residence times lead to excessive chlorination and formation of completely chlorinated derivatives. The distribution of chlorine inside the reactor also plays an important role in containing the product decomposition. Hence, a complete study of flow and species concentration fields inside the reactor is essential for obtaining optimum product formation.

Detailed kinetic schemes for chlorination involve up to 38 species and 157 reactions,[1,2] whereas the simplified scheme used in this work includes 15 species and 21 reactions.[2] The flow in the coaxial reactor used for chlorination is turbulent, and direct numerical simulations of the fundamental transport equations are rendered impossible by the complex interaction between turbulence and reaction. Simulation strategies invoke one of the two simplifications simplified flow dynamics or global chemistry schemes.[3−5] In the past, simple flow models such as the continuous stirred tank reactor (CSTR), plug flow, and combinations of such simple configurations have been used to study the reactor. These approaches do not account for the effect of turbulence on reaction. In addition, nonidealities in plant reactors, such as reactants with a certain degree of nonpremixedness, can only be qualitatively taken into account using nonideal CSTR and other models with increasing complexity. Moreover, in the limit of completely nonpremixed feed streams, reactor runaway is

* To whom correspondence should be addressed. E-mail: rvenkat@iastate.edu.

10.1021/ie0206599 CCC: $25.00
Published on Web 02/05/2003

possible and can only be accurately analyzed using a detailed flow model. Gas-phase chlorination kinetics are similar to combustion chemistry and involve highly exothermic processes. Industrial reactors are usually operated at 2−3 atm, and in the event of a high degree of chlorination, formation of soot is possible through complete decomposition of the hydrocarbons at high temperatures. Models employing simplified flow assumptions cannot predict these conditions accurately.

In the past, the use of more complete flow models has required that the numerical stiffness associated with the free-radical kinetic mechanism be reduced. Several global mechanisms involving a reduced number of species with multistep reactions have been used in two- or three-dimensional geometries with limited success.[4,5] Most of these schemes assume that the inlet has completely premixed reactants. The reaction scheme, in itself, exhibits nonlinear behavior that can lead to instabilities. Studies using a CSTR model show the presence of a Hopf bifurcation point near the ignition branch of the stability curve.[3] Such instabilities have not been corroborated by non-zero-dimensional reactor models. The presence of large numbers of radicals that are essential for accurately predicting reactor behavior also makes convergence of computational fluid dynamics (CFD) simulations difficult because of the wide range of time scales of the reactions. Grid-based Eulerian finite-volume (FV) codes are found to be intractable because of the stiff set of equations involved.[6] Use of a Lagrangian or Eulerian particle-based solution of the joint velocity-scalar probability density function (PDF) transport equation has become prevalent for this type of system.[7] The unstable nature of the velocity transport equations for particle-based methods has led to the use of hybrid FV−particle codes.[8,9] These codes employ a particle-based algorithm to simulate the joint composition PDF and a standard FV code to compute the velocity and turbulence fields. The main advantage of these hybrid schemes is that the reaction terms appear in closed form and require no modeling. The use of joint composition PDF methods for chemical reactors with constant-density flow has been tested elsewhere.[10] A similar scheme with no feedback to the FV code (i.e., one-way coupling) has been used to study a gas-phase premixed chlorination reactor.[11] It was shown that the use of the closed source terms leads to a considerable decrease in the outlet temperature and a consequent increase in the product chloroform fraction. It was also concluded that, to study reaction configurations with highly exothermic reactions (e.g., nonpremixed feed), feedback to the FV code to correct for density changes due to heat release is important. Thus, we have extended the hybrid Lagrangian particle−FV code to account for two-way coupling. A code validation study has been carried out for a turbulent nonpremixed flame,[12] and generally excellent agreement with experimental data was obtained.

In this paper, we apply the hybrid code to study the effect of feed-stream mixing on the exothermic chlorination reactor. Methyl chloride and methyl dichloride are grouped as the organics and are considered as separate from the chlorine stream. As in our earlier work,[11] the jet-stirred reactor has two coaxial inlets. The two streams can be premixed or passed separately in each of these inlets. This setup leads to three different configurations that are analyzed. The rest of the paper is arranged as follows. Section II discusses the mathematical formulation and explains the solution procedure. Then, the numerical scheme is discussed in section III, and changes required for simulating this reactor are noted. Reactor conditions and simulation details are explained in section V, followed by a discussion of the three different feed-stream configurations. Comparisons are also made with simulations using infinitely fast micromixing (i.e., neglecting subgrid concentration fluctuations). Conclusions are drawn about the reactor behavior and simulation methods in section VI.

II. Description of Models

In this work, a hybrid FV−Lagrangian PDF code is used to study the flow and concentration fields inside a jet-stirred reactor. A brief overview of the compressible flow model used in the FV code is given below, followed by a short description of the composition PDF model. More details on both models can be found elsewhere.[13−17]

A. Compressible Flow Model. Using standard notation for mean flow quantities ($\bar{\rho}$, $\bar{p}$, $\tilde{T}$, $\tilde{h}$, and $\tilde{u}_\beta$ are the Reynolds-averaged mean density and pressure and the Favre-averaged temperature, enthalpy, and Cartesian velocity components, respectively) and neglecting body forces and external heat sources, the conservative Reynolds-averaged Navier−Stokes (RANS) equations for the flow of a compressible fluid can be written in a generalized frame of reference $\xi_\alpha = \xi_\alpha(x_\beta)$ ($\alpha, \beta = 1, 2, 3$) as

$$J\left(\frac{\partial \mathbf{Q}}{\partial t} + \mathbf{\Gamma}\frac{\partial \mathbf{W}}{\partial \tau}\right) + \frac{\partial \mathbf{H}_\alpha}{\partial \xi_\alpha} = 0 \tag{1}$$

where J is the Jacobian of the transformed coordinates with respect to the physical frame of reference and repeated indices imply summation (e.g., $A_\alpha B_\alpha = A_1B_1 + A_2B_2 + A_3B_3$). The quantity $\mathbf{Q} = [\bar{\rho}, \bar{\rho}\tilde{u}_\beta, \bar{\rho}E]^T$ represents the vector of conserved variables with E as the total specific internal energy, and $\mathbf{W} = [\bar{p}, \tilde{u}_\beta, \tilde{T}]^T$ is the vector of dependent variables, which includes the pressure, velocity components, and temperature. A pseudo-time term (τ) is added for low-Mach-number preconditioning, and $\mathbf{\Gamma}$ represents a suitable preconditioner.[18] The vector $\mathbf{H}_\alpha$ is the inviscid and viscous flux difference in the ξ_α coordinate direction

$$\mathbf{H}_\alpha = \mathbf{F}^I_\alpha - \mathbf{F}^V_\alpha = J\begin{pmatrix} \bar{\rho}\tilde{U}_\alpha \\ \bar{\rho}\tilde{u}_\beta\tilde{U}_\alpha + \bar{p}\dfrac{\partial \xi_\alpha}{\partial x_\beta} \\ \tilde{U}_\alpha(\bar{\rho}E + \bar{p}) \end{pmatrix} - J\begin{pmatrix} 0 \\ \sigma_{\beta\gamma}\dfrac{\partial \xi_\alpha}{\partial x_\gamma} \\ (\bar{u}_\beta\sigma_{\beta\gamma} + q_\gamma)\dfrac{\partial \xi_\alpha}{\partial x_\gamma} \end{pmatrix} \tag{2}$$

The stress tensor is defined as $\sigma_{\alpha\beta} = -2\mu(S_{\alpha\beta} - {}^1/_3 S_{\gamma\gamma}\delta_{\alpha\beta})$ with

$$S_{\alpha\beta} = \frac{1}{2}\left(\frac{\partial \tilde{u}_\alpha}{\partial \xi_\gamma}\frac{\partial \xi_\gamma}{\partial x_\beta} + \frac{\partial \tilde{u}_\beta}{\partial \xi_\gamma}\frac{\partial \xi_\gamma}{\partial x_\alpha}\right) \tag{3}$$

The quantity $\tilde{U}_\alpha$ is the contravariant velocity: $\tilde{u}_\beta\, \partial\xi_\alpha/\partial x_\beta$. q_α is the total heat flux, written as $q_\beta = (k + \mu_t C_p/Pr_t)\, \partial\tilde{T}/\partial x_\beta$. The thermal conductivity k is calculated from the laminar viscosity and Prandtl numbers; Pr_t is the turbulent Prandtl number, set equal to 0.9 for the present study; C_p is the specific heat, which is calculated

Table 1. List of Variables Solved by the FV and PDF Code[a]

equation	FV	PDF
momentum	$\tilde{\mathbf{u}}$	–
turbulence	$\tilde{k}$, $\tilde{\epsilon}$	–
pressure	$\bar{p}$	–
energy	–	T
species	–	ϕ

[a] Molecular weight W and mean temperature $\tilde{T}$ can be computed from the PDF variables.

from polynomial fits according to temperature; and μ_t is the turbulent eddy viscosity.

The inviscid flux, $\mathbf{F}^I$ is separated into convective and pressure components using a second-order, low-diffusion flux-splitting scheme (LDFSS).[19] Second-order backward three-point physical time differencing is used for the time-dependent term, Euler differencing is used for the pseudo-time derivative, and second-order central differences are used for the viscous terms. The system is closed using the ideal gas law, $\bar{p} = \bar{\rho}R\tilde{T}/W$, where W is the molecular weight of the gas mixture. It should be noted that the energy equation is not solved to determine the enthalpy or temperature, which are directly obtained from the PDF code (described below) and remain "frozen" during the FV iterations. The energy equation is retained as part of the original FV formulation and is not needed in the hybrid code. The temperature values are used to calculate thermophysical properties of the fluid. Equation 2 is linearized, and the resulting system is solved using a fully implicit multigrid-level line relaxation scheme. In the multilevel scheme, the system is solved on increasingly finer grids, interpolating the solution from coarser grids. However, the PDF code is restricted to the finest grid. Transport equations for the Favre-averaged mean turbulent kinetic energy $\tilde{k}$ and dissipation rate $\tilde{\epsilon}$ are solved as a separate coupled system. The standard two-layer form of the model is used.[20]

In the present work the above system is solved for a single constituent with a spatially varying molecular weight to obtain the velocity ($\tilde{\mathbf{u}}$) and turbulence quantities ($\tilde{k}$ and $\tilde{\epsilon}$). Using these flow quantities, the PDF code is employed to obtain a new temperature ($\tilde{T}$), density $\bar{\rho}$, and molecular weight (W), which are fed back to the RANS code to update the velocity and turbulence fields. Table 1 lists the variables solved by each code. This loosely coupled RANS–PDF solution procedure is described in more detail next.

B. Lagrangian PDF Model. The velocity and turbulence models have been solved for a variety of flows on complex geometries. For reacting flows, the stiffness in the system is mainly due to the presence of the species reaction source terms. For a large chemistry mechanism involving strong temperature dependence, the species transport equations form a stiff system that requires very small time steps dependent on the reaction time scales. In the case of the chloromethane scheme, it has been found that the time scales vary by over 8 orders of magnitude. Simplification of the chemistry can lead to large errors in the CFD predictions. In such situations, the PDF formulation of the scalar transport equation combined with in situ adaptive tabulation (ISAT)[21] provides a tractable scheme. If the molecular transport coefficients for all species and temperature are taken to be equal and constant (Γ), the composition PDF obeys the following equation[22]

$$\frac{\partial \bar{\rho}\tilde{f}_\phi}{\partial t} + \frac{\partial}{\partial x_i}(\rho\tilde{u}\tilde{f}_\phi) + \frac{\partial}{\partial x_i}[\bar{\rho}\langle u_i'|\psi\rangle\tilde{f}_\phi] = -\frac{\partial}{\partial \psi_i}[\bar{\rho}\langle\Gamma\nabla^2\phi_i'|\psi\rangle\tilde{f}_\phi] - \frac{\partial}{\partial \psi_i}[\bar{\rho}(\Gamma\nabla^2\tilde{\phi}_i(\psi) + S_i(\psi))\tilde{f}_\phi] \quad (4)$$

where $\langle\cdot\rangle$ refers to the density-weighted mean and $\tilde{f}_\phi = \rho f_\phi/\bar{\rho}$ represents the density-weighted joint composition PDF with the property

$$\int_{-\infty}^{+\infty} \tilde{f}_\phi(\psi;\mathbf{x},t)\, d\psi = 1 \quad (5)$$

Integration of eq 4 over composition phase space yields the transport equation for the mean density $\bar{\rho}$. Likewise, multiplication by ψ_i and integration over composition space yields the transport equation for $\bar{\rho}\bar{\phi}_i$. The chemical source term is denoted by S, and the density-weighted scalar-conditioned expected value by $\langle\cdot|\psi\rangle$. It can be noted that the source term for the reaction in eq 4 appears in closed form and needs no modeling. However, the subgrid-scale mixing term ($\langle\Gamma\nabla^2\phi_i'|\psi\rangle$) must be described by a micromixing model. Likewise, the scalar flux term due to velocity fluctuations $\langle u_i'|\psi\rangle$ can be closed by invoking a turbulent-diffusion model that is consistent with eq 1.[23] In this work, we use $\bar{\rho}\langle u_i'|\psi\rangle\tilde{f}_\phi = -(\mu_t/Sc_t)\ \partial\tilde{f}_\phi/\partial x_i$, where Sc_t is the turbulent Schmidt number assumed to be a constant equal to 0.7.

The coefficients in eq 4 involve mean fields obtained from the solution to the compressible flow model. As explained earlier, the flow field is generated using a traditional FV scheme. The PDF transport equation is then solved using detailed chemistry to obtain the mean temperature ($\tilde{T}$) and molecular weight (W) fields. These are then used along with the ideal gas law to provide the density correction to the flow solver. The iterative process is repeated until convergence is obtained. It should be noted that the PDF transport equation itself is in (N + 3) dimensions for an N-species, three-dimensional problem. Finite-differencing schemes are not feasible for more than one or two scalars. A stochastically equivalent system with a large number of notional particles is used to evolve the PDF according to the PDF equation.[10,24–26] There are several variations to the solution scheme for a hybrid method. The use of a joint velocity, composition PDF is common where particle equations are formulated for the velocity fields also.[16,27] Statistical noise in the solution fields might lead to instabilities in such schemes. Here, the PDF equations are simplified to represent only the joint scalar statistics. The PDF solution method can itself be formulated in an Eulerian[8] or a Lagrangian[10] frame. In the former approach, the particles are confined to cell nodes, and transfer of particles is based on fluxes across cell faces. This is simple to implement but introduces numerical diffusion.[28] Eulerian schemes are found to be better suited for problems that have a predominant flow direction. For the jet-stirred reactor, the presence of a recirculation zone renders the Lagrangian formulation more effective.

In the Lagrangian scheme, the stochastic particles are distributed evenly over the entire domain and are transported in physical and composition space using particle transport equations consistent with eq 4.[27] The particle transport algorithm uses mean fields of velocity and turbulence from the FV solution. Transport in physical space is handled by the particle-position stochastic differential equation

$$d\mathbf{x}^* = \left[\tilde{\mathbf{u}}(\mathbf{x}^*,t) + \frac{1}{\bar{\rho}(\mathbf{x}^*,t)}\nabla\bar{\rho}(\mathbf{x}^*,t)\,\Gamma_{\text{eff}}(\mathbf{x}^*,t)\right] dt + \sqrt{2\Gamma_{\text{eff}}(\mathbf{x}^*,t)}\, d\mathbf{W}(t) \quad (6)$$

where the coefficients are estimated using the mean flow fields at the particle position. The effective diffusivity (Γ_{eff}) is the sum of the molecular and turbulent diffusivities obtained by

$$\Gamma_{\text{eff}} = \Gamma + \frac{\mu_t}{\bar{\rho} Sc_t} \quad (7)$$

where μ_t is given by

$$\mu_t = \frac{C_\mu \bar{\rho}\tilde{k}^2}{\tilde{\epsilon}} \quad (8)$$

with C_μ being 0.09. The "noise" term, $d\mathbf{W}(t)$, is a multivariate Wiener process with mean zero $\langle dW_i(t)\rangle = 0$ and covariance structure $\langle dW_i(t)\, dW_j(s)\rangle = \delta_{ij}\delta(t-s)\, dt$.

The transport in composition space consists of two substeps: reaction and micromixing. The reaction substep is described by a set of coupled ordinary differential equations for the N species

$$\frac{d\phi^*}{dt} = \mathbf{S}(\phi^*) \quad (9)$$

Though mathematically simple, a full PDF simulation requires at least 10^9 computations of the solution to this equation, which makes the simulation intractable for large N. The use of precomputed lookup tables and low-dimensional manifolds[29] is not feasible solutions for large chemistry mechanisms. As in our previous work,[11] ISAT is used here and provides a powerful alternative to direct integration of eq 9. With improved storage of the accessed region in composition space (as opposed to the entire composition space in precomputed lookup tables), ISAT increases the computational speed by factors of up to 100 over direct integration of the source term. The validity of ISAT for chlorination chemistry has been tested elsewhere.[2]

One of the other advantages of the PDF method is that a micromixing model can be used to describe scalar fluctuations in the fluid at the subgrid scale. Several mixing models have been formulated, although the coalescence−dispersion, IEM,[30] and binomial Langevin[31] models are the most commonly used. Here, the IEM (interaction by exchange with the mean) model is used. The IEM model assumes that the mixing rate is linearly proportional to the distance from the mean in composition space. The proportionality coefficient is constant and is determined by the local turbulence characteristics. The micromixing substep can then be expressed as

$$\frac{d\phi^*}{dt} = \frac{C_\phi \tilde{\epsilon}}{2\tilde{k}}(\tilde{\phi}(\mathbf{x}^*,t) - \phi^*) \quad (10)$$

where C_ϕ has a nominal value of 2 and $\tilde{\phi}(\mathbf{x}^*,t)$ is the estimated mean scalar at the particle location. The IEM mixing model is known to be inaccurate for certain homogeneous nonpremixed flows, but it often provides an adequate representation of subgrid-scale fluctuations for inhomogeneous flows. Other more complex models exist but are computationally expensive and have been successfully used only in select cases. In the PDF simulations, eq 10 is solved first using the current particle compositions as the initial condition. The results from this substep are then used as the initial conditions to solve eq 9.

The temperature or enthalpy equation is solved by the particle algorithm. In essence, the effect of chemical reactions is fed back to the FV code in the form of the temperature and molecular weight fields, which are then used to correct the flow for reaction by computing the density. The nature of the feedback can be tight or loose, depending on the frequency of FV and PDF interactions. In this work, a loosely coupled algorithm is implemented in which a steady-state FV solution is corrected by the particle code every M steps, where M is an arbitrarily fixed number (set to 10 in this paper). Usually, a sufficiently large M is chosen so that time averaging of the statistically noisy temperature field can be carried out. In the limit of tight coupling ($M = 1$), feedback is implemented with an unsteady FV solver at each time step and is usually unstable unless a large number of stochastic particles is used, along with a small time step.

III. Overview of Simulation Algorithm

The FV code, as explained earlier, provides the mean flow fields as well as the turbulence fields. In theory, the velocity fields must be mass-conserving.[16] This will ensure that the particles, which are uniformly distributed at the start of the simulation, will remain uniformly distributed. However, in many reacting flow problems, the high temperature and other flow gradients lead to small mass imbalances in the velocity fields. This leads to particle accumulation that is proportional to the errors in the discrete form of the continuity equation. Particle position and velocity correction techniques have been proposed[16] for structured grids. In this work, the particle weights were adjusted uniformly during each feedback step to account for slight deviations from the continuity balance.[12]

As explained in the previous section, the Monte Carlo method involves tracking a large ensemble of notional particles through the flow domain. Particle tracking is nontrivial for nonorthogonal and clustered grids, and an efficient cell-based particle tracking scheme is employed in the PDF code.[22] The face normal vectors for a cell are used to compute the time required by the particle to reach each of the faces of the cell. The individual particles are then moved to the face that requires the shortest time. After this step, particle control is transferred to the neighboring cell, which moves the particle across its domain according to the local mean fields. This piecewise procedure is repeated until the global time step is reached. Steep temperature gradients induce sharp changes in local properties, and hence, particle values have to interpolated according to local cell properties. The tracking scheme is independent of the grid, and the computational time is found to increase linearly with the number of particles. This method overcomes the limitations in time step imposed by the clustering of grid points required to resolve steep gradients. The global time step is limited only by the local micromixing times, instead of by the local mean particle residence time in the cell.

In the case studied here, an axisymmetric grid is used where the cell volume is proportional to the distance from the centerline of the grid. The notional particles in a cell are representative of the cell mass, and each particle carries a normalized weight. At the start of the

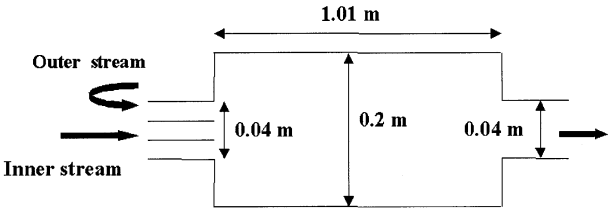

Figure 1. Schematic representation of reactor.

simulation, the particles are uniformly distributed in the domain and are assigned weights proportional to the local cell mass (i.e., the cell volume multiplyed by the cell mean fluid density). In the course of the simulation, particles of varying weights can enter a particular cell, leading to loss of uniformity of particle number density. Because this can adversely affect the statistical accuracy of the mean-field estimates, a process of particle clustering and breakup[15] is initiated to conform particles to the local cell mass and, at the same time, maintain particle number density within a small range. Note that, at any time step, the mean density field predicted by the PDF code can be computed by summing the particle weights in each cell. This field can be compared to that found from the FV solver ($\bar{\rho}$). The ability of the PDF code to maintain consistency with $\bar{\rho}$ can be used to check the accuracy of the particle tracking and interpolation algorithms. A well-written hybrid FV, PDF code should be able to maintain consistency within a few percent.

The mean fields from the PDF code are computed using all of the particles in a given cell. In addition, the fields are time-averaged over a fixed number of steps before being fed back to the FV solver. It was found that an average of 100 particles per cell must be used for all of the simulations to reduce statistical bias.[17] The number of feedback iterations was arbitrarily fixed at 10 after trial and error. This ensures that the changes in the temperature fields are not large enough to cause

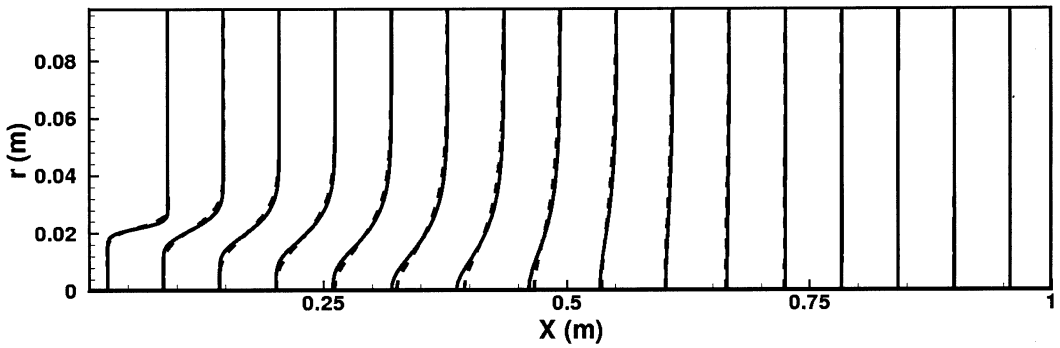

Figure 2. Radial temperature profiles for different grid sizes at various axial positions. The solid lines represent a 53 × 33 grid, and the dashed lines represent a 53 × 79 grid. The temperature has been normalized with respect to an arbitrary value of 750, and the maximum axial shift is 0.05 m for this temperature.

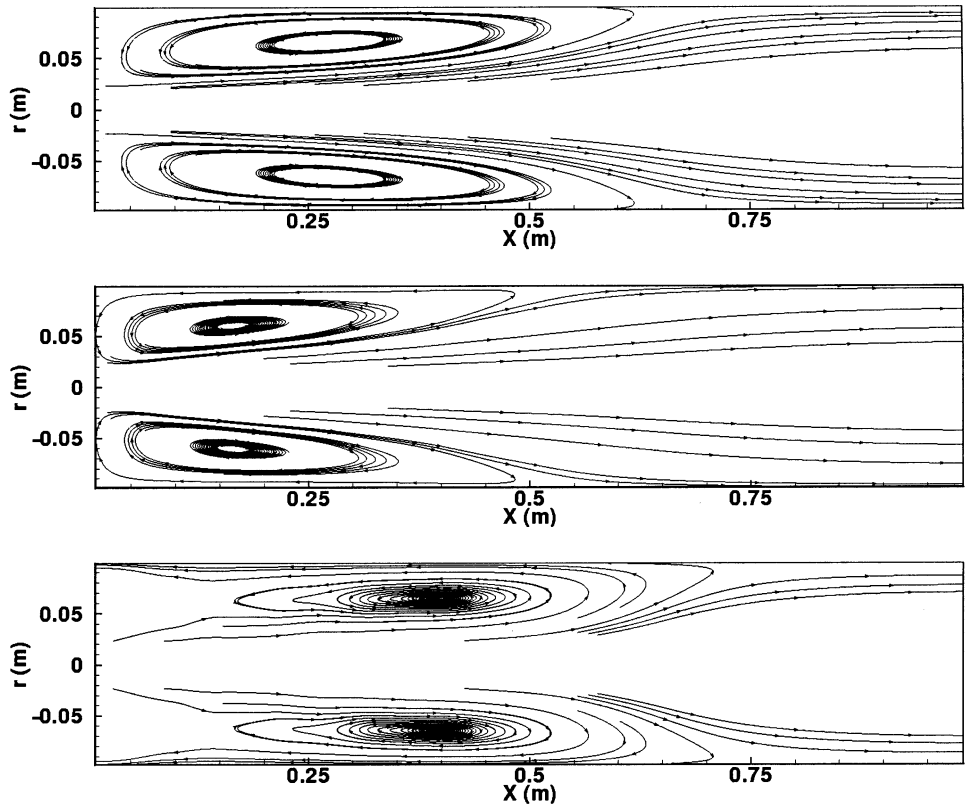

Figure 3. Streamlines illustrating recirculation zones for (top) premixed, (middle) nonpremixed with chlorine inner jet, and (bottom) nonpremixed with chlorine outer jet configurations.

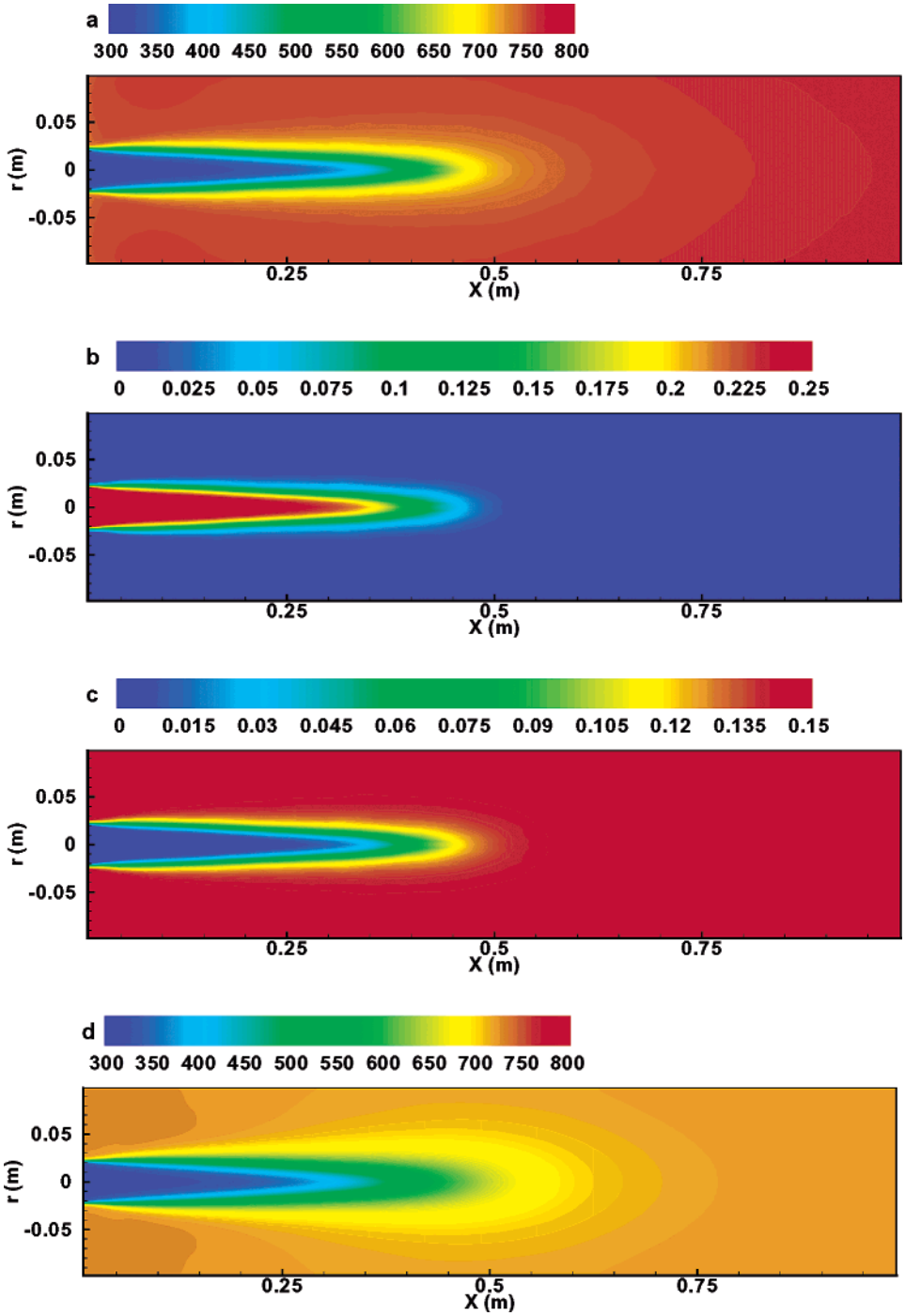

Figure 4. Profiles of (a) temperature, (b) chlorine, and (c) chloroform for the premixed case. (d) Temperature profile with infinitely fast micromixing.

the FV solver to diverge. As discussed earlier, temperature and molecular weight are used as the feedback variables. Using the pressure field from the FV solver, the mean density is computed to close the equations. The FV solver then iterates for approximately 2500 steps with the pseudo-time step term driven down using a variable CFL number.

IV. Reactor Simulation

The coaxial jet-stirred configuration (Figure 1) provides good mixing of the reactants with a high shear layer at the interface of the two jets. In this work, we investigate the effect of inlet stream configuration (e.g., premixed vs nonpremixed) on reactor performance for fixed inlet mass flow rates. Thus, for all of the simulations, the inlet organic stream has a composition of 48% methyl chloride and 52% methyl dichloride with a mass flow rate of 0.028 44 kg/s. The inlet chlorine stream has a flow rate of 0.009 36 kg/s. In the premixed case, the reactants are assumed to be completely mixed at the above mass flow ratios before entering the reactor. (In our earlier work, a pilot-scale reactor was simulated using a constant-density PDF method with premixed inlet.[11]) In this work, the jet diameters are adjusted such that the inlet velocity of the streams is equal to 3.01 m/s for both the premixed and nonpremixed cases. (The effect of unequal velocities are being studied and will be reported elsewhere.) The inlet temperature of both

streams is set to 323 K. Although pilot-scale experimental studies show reactor stability, nonideal CSTR studies with the same residence time (≈7.5 s) and inlet temperature show a high probability for reactor extinction. The coaxial reactor has a characteristic recirculation zone between the inlet and the wall that provides near-complete mixing. Also, the recirculation zone helps to transport back enthalpy to the incoming cold fluid to sustain the reaction. (In the limit of plug flow, it can easily be shown that the reactor will not stay lit.)

Orthogonal uniform grids were used for the premixed case. A grid-independence study was carried out using a 53 × 33 mesh and a 53 × 79 mesh. Radial temperature profiles at different axial positions for the two cases assuming infinite-rate mixing conditions are shown in Figure 2. The time-averaged fields for different grid resolutions show very little difference. The smaller grid size was chosen for all cases reported in this paper. The nonpremixed cases were found to have steep temperature gradients, and hence, grid clustering was necessary near the inlets. However, the overall mesh size was retained for the sake of comparison.

A reduced mechanism with 15 species and 21 reactions[11] was used in this work. It has been noted elsewhere that the use of a larger 38-species mechanism does not fundamentally alter the behavior of the reactor but offers some quantitative differences. Because the thrust of this paper was to study the effect of inlet configuration, the reduced mechanism was found to be sufficient. It should be noted that the simulations could be repeated for the detailed chemistry mechanism without modifying the hybrid FV−PDF code. The only appreciable difference would be the proportion of CPU time needed by ISAT to treat the chemistry.

For the nonpremixed case with chlorine in the inner stream, the jet diameters were the same as for the premixed case. In the other nonpremixed case, where the organics with a higher mass flow rate were in the inner stream, the inner-jet diameter was increased to 0.034 m and the outer-jet diameter was kept the same (0.04 m). For each of these cases, two conditions were studied. In the first (finite-rate micromixing), the IEM model (eq 10 with $C_\phi = 2$) was used based on the local turbulence field. In the other (infinite-rate micromixing), complete micromixing was assumed ($C_\phi = \infty$). The latter is equivalent to an FV solution with no subgrid closure for micromixing. The overall time step was set according to the minimum micromixing time for a nonreacting flow field. Chemical reactions usually lead to an increased rate of micromixing (due to changes in the flow field) and a consequent decrease in the variance of the scalars. However, it was noticed that the change in the minimum micromixing time was quite small, thereby validating the choice of the time step. In the finite-rate micromixing cases, the time step was set to 2×10^{-3} s. For studies with infinite-rate micromixing, the time step was increased to 1×10^{-2} s. Because of the absence of micromixing, the time step for this case was controlled by the reaction and the error caused by fractional time stepping. It was found that smaller time steps yielded no differences in the solution.

V. Simulation Results

The jet-stirred reactor simulations were carried out on a single processor on a 900-MHz SUNFIRE machine. It was found that reaction source term calculations took nearly 93% of the computational time. To minimize CPU time, the simulations were carried out in three stages. Initially, a nonreacting flow field was generated, and the PDF code was run with complete micromixing ($C_\phi \gg 1$) with no temperature feedback. Using the converged scalar fields, feedback was initiated, and the flow field converged. In the final stage, the micromixing model was turned on ($C_\phi = 2$), and the simulation continued for 1.5−2.0 residence times. It was found that this strategy provided a stable solution with an approximately 45% reduction in computational time as compared to starting the simulation with all physical processes activated. The streamlines for the three configurations are shown in Figure 3. The effect of recirculation on flow for each inlet configuration is discussed below.

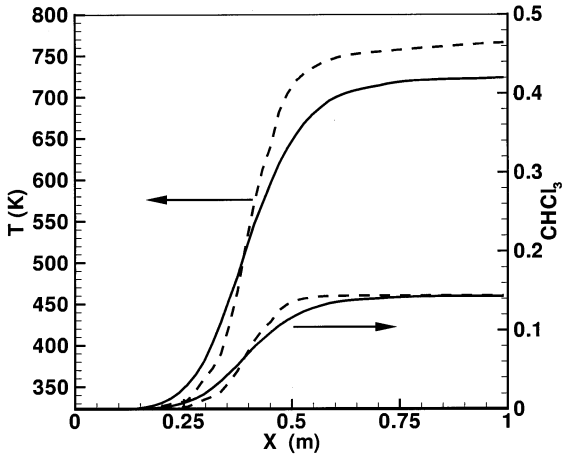

Figure 5. Centerline temperature and product profile for (solid) infinitely fast micromixing case and (dashed) IEM mixing model with premixed inlets.

For the nonpremixed case, the scatter plots of scalar values conditioned on the mixture fraction are used for analysis. The definition of mixture fraction used is

$$\xi = \frac{Y_C - Y_{C1}}{Y_{C2} - Y_{C1}} \tag{11}$$

where Y_C refers to the mass fraction of elemental carbon and the subscripts 1 and 2 refer to the mass fractions of carbon in the two inlet streams. In the case of a nonpremixed inlet, a value of 0.1753 is used for the organic stream carbon content (Y_{C2}), and the pure chlorine stream (Y_{C1}) has a carbon mass fraction of 0.0. This normalizes the mixture fraction to vary from 1.0 for the organic stream to 0.0 for the pure chlorine stream.

A. Premixed Inlet. For this case, both inlet streams contain 25% chlorine, 36% methyl chloride, and 39% methyl dichloride (percentage based on total mass). The profile of the temperature (Figure 4a) shows a flame-like structure with a maximum temperature of 752 K. Because chlorination involves the formation of free chlorine atoms, the penetration of chlorine (Figure 4b) inside the reactor to a large degree determines the efficiency of the reactor. The residual chlorine free radical shows the region of reaction to be situated in the thin diffusion layer surrounding the jet. The chlorine molecules disassociate because of the higher temperature in this region. There is a competitive reaction between carbon tetrachloride and chloroform with the concentration profiles following the temperature profile (Figure 4c). The formation of organic free radicals leads

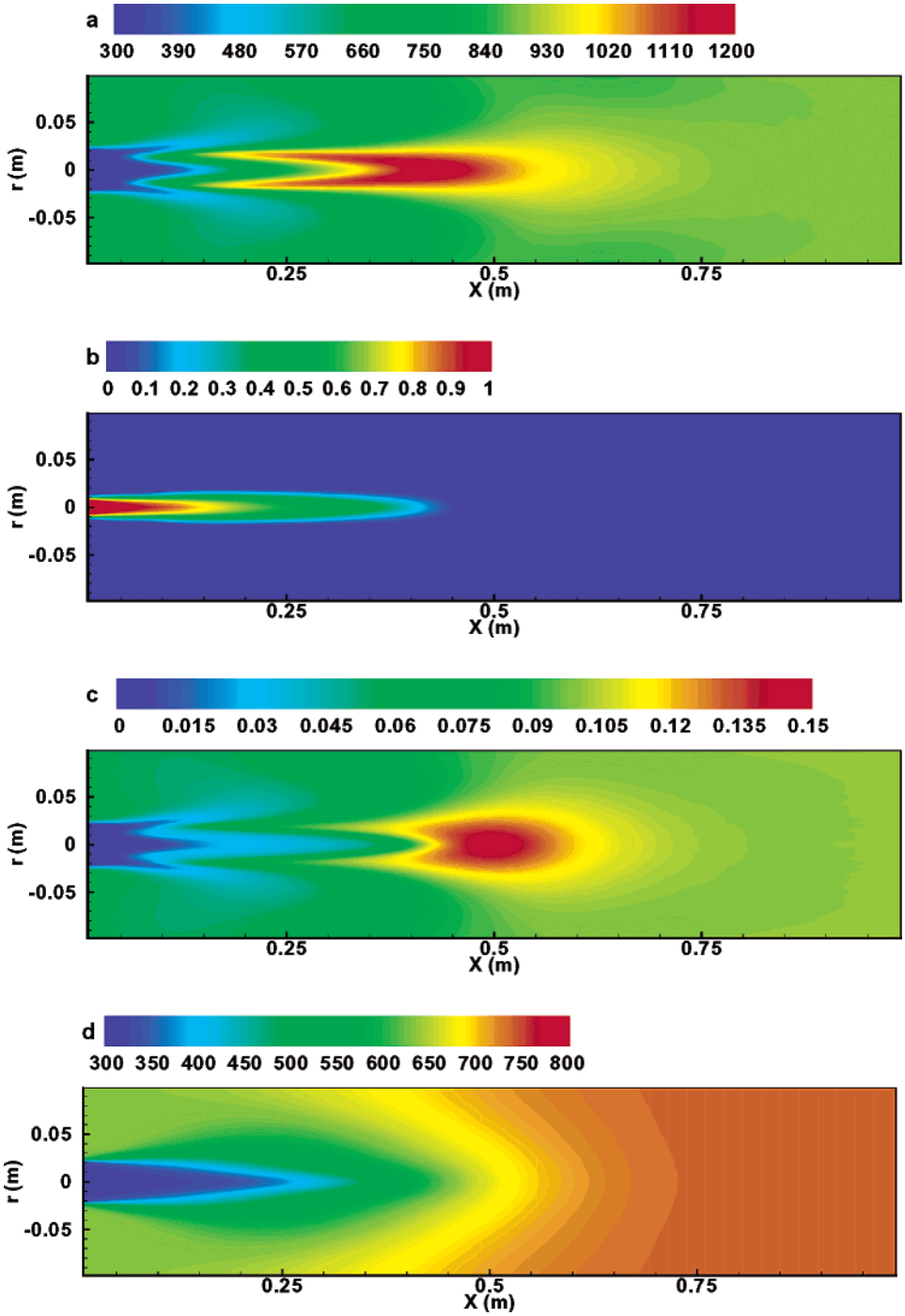

Figure 6. Profiles of (a) temperature, (b) chlorine, and (c) chloroform for the nonpremixed case with chlorine as the inner jet. (d) Temperature profile with infinitely fast micromixing.

to quenching in the outer layers of the reaction zone. This region contains product contamination by tertiary chlorination. The highly exothermic nature of the reactions leads to a large temperature rise that gets carried back into the recirculation zone (Figure 3a). The increase in temperature also tends to push the gases out of the reactor. This reduces the effective residence time of the reactants in the main stream, thereby reducing the reaction and decreasing the temperature. Eventually, an equilibrium is reached where chlorine conversion is complete and the enthalpy increase is kept in check by expanding gases that increase the mean flow velocity.

It has been observed[11] that, even when the temperature feedback is absent, the structure of the flame can be predicted quite accurately. The constant-density simulation performed previously produces very similar temperature and product profiles. However, the feedback to the FV solver changes the reattachment point and thereby affects the volume of fluid trapped in the recirculation region. Greater reattachment lengths might lead to dilution of enthalpy and result in global extinction. In essence, the stability of the reactor is controlled by the residence time in the recirculation region rather than by the global flow rate. The premixed case is stable to the point that changes in reattachment length are compensated by reaction dilution or increase to maintain the ignited state of the reactor.

The case with infinite-rate micromixing does not significantly change the product distribution (Figure 4d)

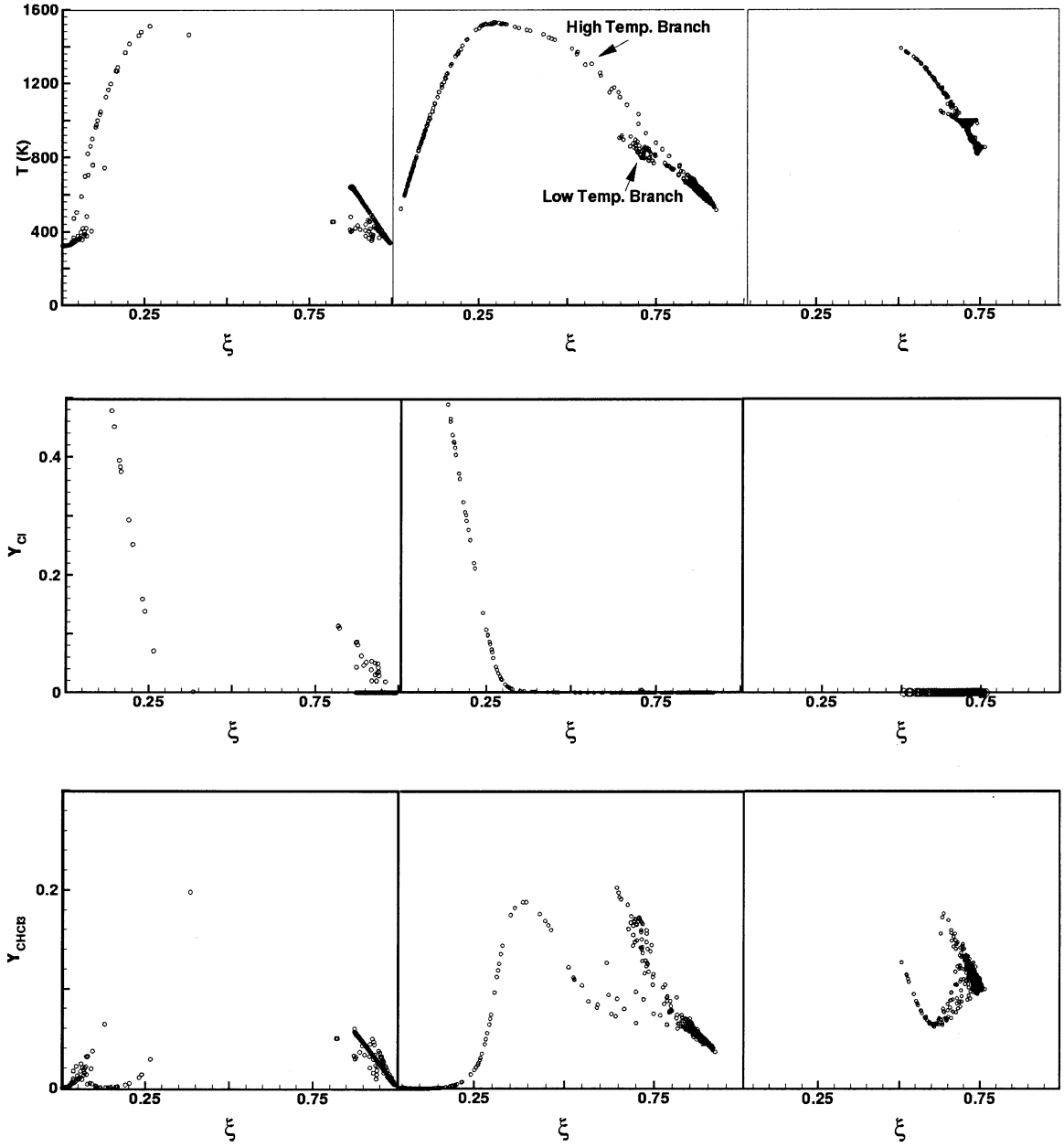

Figure 7. Radial scatter plots at different axial distances of (a) temperature, (b) chlorine, and (c) chloroform for the nonpremixed case with chlorine as the inner jet. Starting from the left, the figures in each column correspond to axial positions of $x/r = 1$, $x/r = 3$, and $x/r = 6.7$, respectively.

and shows a similar flame structure. It should be noted that the chlorine is not completely consumed and a residual fraction on the order of 10^{-4} is present at the outlet. This explains the decrease in outlet temperature to about 720 K (Figure 5). The chloroform yield is only slightly different, mainly because of decreased chlorination in the reaction layer (Figures 4d and 5). The excess chlorine free radical is now limited to the region of interaction with the recirculation zone. The end of the flame has no free radicals, showing complete consumption of disassociated chlorine. Also, the reaction layer is very diffuse and extends deeper into the recirculation region. The chloroform yield is uniform across the outlet at 14% by mass.

B. Chlorine in the Inner Jet. In this case, the reactants are separated, and the chlorine stream is fed through the inner jet. The temperature profile (Figure 6a) shows that the reaction zone has now been shifted to the end of the jet core. This is quite evident considering the fact that a high degree of mixing is required to get sustainable reaction. The chlorine profile (Figure 6b) follows that of a simple jet but is shortened because of the high temperature gradients arising from reaction. The end of the jet has almost completely mixed particles that yield temperatures as high as 1500 K. The reaction zone, which is detached from the jet core, has a "two-pronged" structure because of the entrainment of the outer cold streams in the recirculation zone. It can be noted that the peak in the chloroform mass fraction is found downstream of the peak in the temperature. This is mainly due to the higher decomposition rates that increase with temperature. One of the distinct differences from the premixed case is that the recirculation zone does not carry all of the enthalpy generated from the reaction. The reaction layer is located at the end of the entrainment zone, leading to limited heat recirculation (Figure 3b). In fact, this acts as the stabilizing factor, preventing excessive reaction in the jet core that

might lead to reactor runaway. Movement of the reaction further downstream will cut off enthalpy feedback leading to reactor extinction. Hence, this configuration is inherently unstable, and minor disturbances in inlet stream properties can lead to extinction. The reaction layer itself is drawn out axially as a result of the expansion caused by the temperature rise. The higher temperatures and consequent product decomposition decrease the chloroform yield to 10% (Figure 6c).

The carbon tetrachloride yield is also restricted to around 1.2%. In the reaction zone, the concentration of chlorine free radical is very high (more than 6 orders of magnitude greater than in the premixed case) and leads to the formation of carbon−carbon bonds with tertiary chlorinated derivatives. It should be noted that this free radical is the excess fraction after consumption in primary chlorination reactions, which indicates the scarcity of organic free radicals that can consume chlorine atoms. The higher temperature leads to further decomposition of chlorine molecules, and a relatively high mass fraction (17%) of hydrogen chloride is formed. The outer zone of the reaction layer also carries a relatively high fraction of organic species, which causes the carbon−carbon bond formation to be favored.

The conditional scalar scatter plots (Figure 7) based on the mixture fraction (eq 11) indicate an interesting feature of the chemistry. The reactions are essentially separated into two branches. The high reaction rates ensure that the scalars are near equilibrium in the reaction zone. In the zone near the inlet (at $x/r = 1$), mixing is limited, and the reaction is limited to particles with high chlorine content. As the jets mix more downstream, higher temperatures (partially due to the feedback enthalpy) lead to local ignition, and almost all of the particles reach the equilibrium curve. It can also be seen that certain particles in the carbon-rich zone fall below this curve, suggesting that the chlorine levels in these particles are not high enough to cause ignition. They are still controlled by the mixing process and will ignite as they move downstream. The chloroform production is at a peak, and the maximum yield is around 20% by mass. It can be seen that the maximum temperatures are found around a mixture fraction of 0.25, which is close to the stoichiometric mixture fraction for maximum chloroform conversion. The chloroform peak lags slightly behind temperature, with the maximum observed in two separate branches in chlorine-rich and carbon-rich zones. At the end of the reaction zone, the chlorine fraction is completely consumed. It should be noted that, because of the ignited state of the reactor, the particle temperatures collapse onto the reacting branch. The chloroform fraction is reduced through secondary reactions to its outlet value.

The infinite-rate micromixing (Figure 8) shows behavior similar to that of the premixed case. The diffusive nature of the infinite-rate micromixing case combined with the shear layer at the interface of the jets leads to a nearly premixed condition, and the rest of the reactor behaves in the same way as the premixed reactor. However, the recirculation zone is cooler than the premixed case because of the lower chlorine content in the feedback stream. The organic layer shields the high chlorine jet from entering the dead zone and keeps the chloroform yield at almost the same level as in the premixed case (Figures 6d and 8). Even though faster mixing leads to higher reaction rates, the rate of dilution of enthalpy prevails, balancing any exothermic release

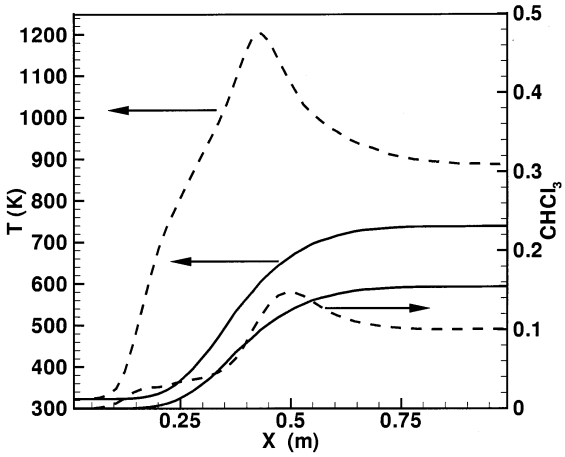

Figure 8. Centerline temperature and product profile using (solid) infinitely fast micromixing condition and (dashed) IEM mixing model for nonpremixed inlets with chlorine in the inner stream.

of heat with a decrease in temperature through mixing with colder inlet streams. Comparing profiles c and d of Figure 6, it is evident that this configuration provides an excellent example of the need for micromixing closures in reacting flow simulations.

C. Chlorine in the Outer Jet. In this case, the organics stream is in the inner jet, and chlorine in the outer jet. The jet diameters have been changed to ensure that the inlet velocities are the same as in the previous cases. The presence of a pure chlorine stream near the recirculation region changes the zone of reaction. The reactions are now confined to the recirculation region and the jet interface that interacts with this zone (Figure 9a). The chlorine stream (Figure 9b) is partially entrained into the recirculation flow and hence creates a "bifurcated" front. Also, complete chlorine consumption is observed within the first 10% of the reactor length. Such short penetration distances have an adverse effect of tertiary chlorination that produces carbon tetrachloride. The depletion of chlorine leads to reaction quenching through carbon−carbon bond formation. The position of the reaction zone causes much of the organic stream to pass through the reactor without reaction (Figure 3c). Even though high temperatures are observed in the reactor, conversion of primary chlorinated derivatives is very low. The chloroform yield (Figure 9c) is around 4%, which is the lowest among the three configurations. The strong mixing conditions present near the chlorine−organics interface keep the reactor lit. The recirculation zone will cause a positive feedback loop with increasing temperatures. However, higher temperatures will lead to faster depletion of chlorine and a reduction in the reaction layer thickness. This will reduce heat release into the recirculation zone and will reduce reaction rates. Such a mechanism is inherently unstable, with slight changes in mixing condition between streams leading to reactor runaway. It should also be noted that the mechanism used here does not account for soot formation. In pilot-scale reactors, at such high temperatures, deposition of carbonic soot on the reactor surface has been observed.

A high level of residual chlorine free radical is produced at the interface of the chlorine stream and the recirculating flow. However, the maximum organic free radical is produced slightly upstream, leading to high reaction rates as these free radicals move into the chlorine stream. The resulting temperatures propel the

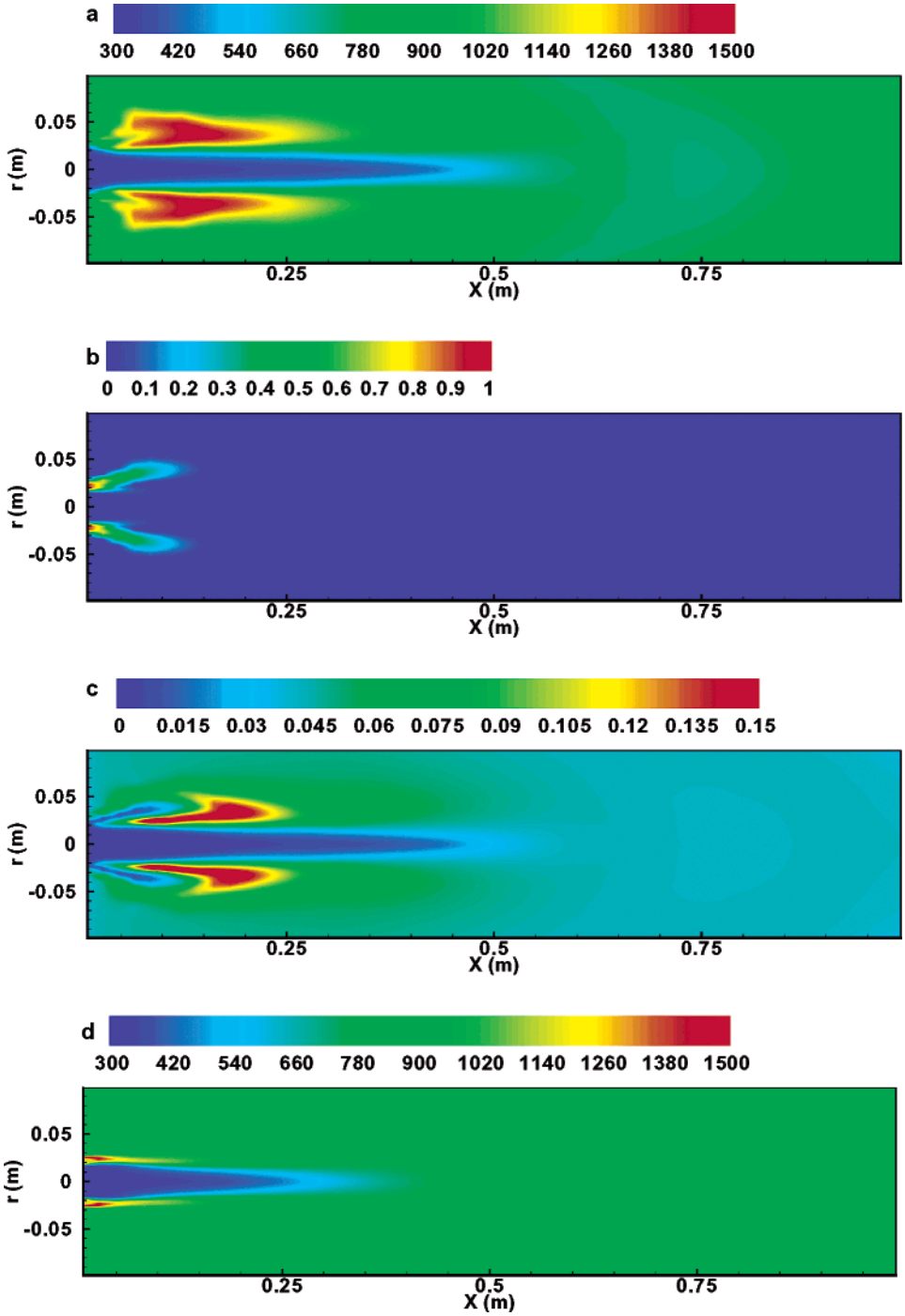

Figure 9. Profiles of (a) temperature, (b) chlorine, and (c) chloroform for the nonpremixed case with chlorine as the outer jet. (d) Temperature profile with infinitely fast micromixing.

reactions toward the high-temperature branch locally. However, such strong reactions are confined to the recirculation zone, and the rest of the reactor is extinct as there is very little transfer of enthalpy and chlorine molecules to sustain reaction. The reaction zone is highly localized, and the reactor state cannot be observed from the centerline species or temperature profiles, the latter being the only data available from a plant-scale reactor. Hence, this reactor constitutes a risk in an industrial scenario.

The scatter plots (Figure 10) show the existence of a distinct reaction branch and a mixing branch. The reactions occur at a higher temperature and are restricted to particles with high chlorine fraction. The chloroform profiles show that a maximum of 28% mass fraction is attained for particles in zones where mixing with cooler nonreacting particles is more probable. This keeps the reacting particles lit and feeds reactants as well. Further downstream, the consumption of chlorine is complete, and the reacting branch collapses to the mixing branch with global extinction around $x/r = 6$. The chloroform plots show that the preferred mass fraction is the lower peak observed in the reacting zone. Higher mass fractions are decomposed to other carbon−carbon-bonded chlorine derivatives. Near the end of the reactor, the reaction branches have collapsed completely onto the mixing branch. The complete depletion of chlorine upstream leaves no reactants, but a high temperature that leads to further decomposition of product.

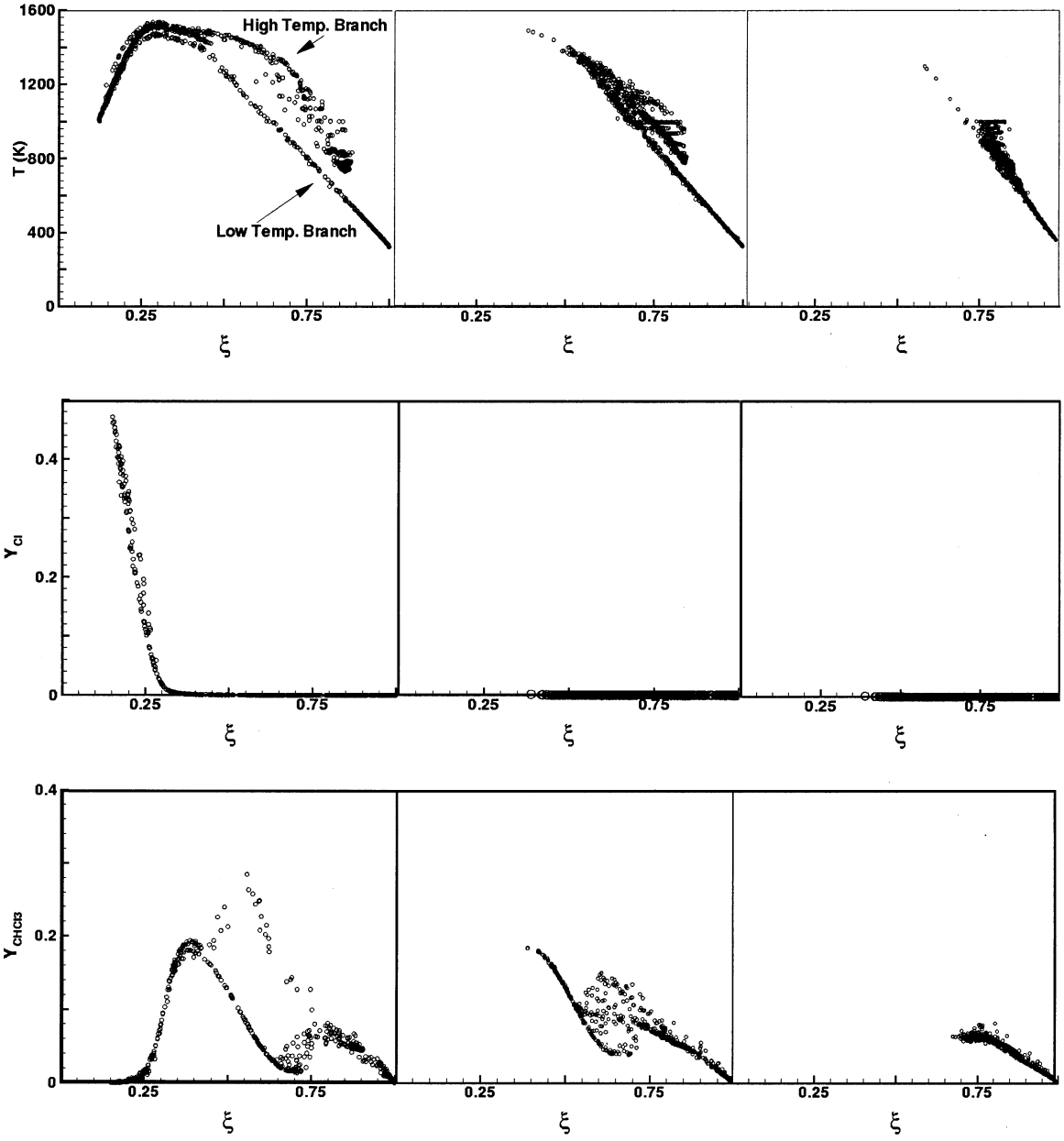

Figure 10. Radial scatter plots at different axial distances of (a) temperature, (b) chlorine, and (c) chloroform for the nonpremixed case with chlorine as the outer jet. Starting from the left, the figures in each column correspond to axial positions of $x/r = 1$, $x/r = 3$, and $x/r = 5$, respectively.

The infinite-rate micromixing case (Figures 9d and 11) shows results different from the previous nonpremixed case. The faster mixing provides for better mixing conditions, thereby spreading the core of the inner jet. This leads to higher temperatures with shorter reaction zones. The peak in temperature occurs near the inlet and away from the centerline with global extinction observed farther downstream. The final outlet temperatures remain almost the same as in the finite-rate micromixing case. As before, product decomposition is very high, and a surge of reactant mass fraction is seen at the end of the reactor. It can be noticed that the centerline temperature profile looks very similar to that in the premixed reactor. CFD simulations with no subgrid-scale closure for the source term will thus yield similar centerline profiles for both the premixed and nonpremixed cases. Evidently, closure in the form of a mixing model is required, although the form of the model that will be the most suitable should be determined on the basis of experimental data.

The centerline temperature for the finite-rate micromixing case shows a sudden increase toward the end of the reactor. This is due to the inherent instabilities in the reactor that cause the reattachment point to vary with time. Such changes lead to "peel-off" of high-temperature layers that are then pushed into the plug-flow zone and carried out of the reactor. However, they are found to have very little effect on the product composition. The frequency of peel-off varied with time and can depend on the frequency of feedback (i.e., M). These results were found with $M \leq 10$, whereas for $M > 100$, the reactor became extinct.

VI. Conclusions

A hybrid finite-volume−joint composition PDF simulation code with detailed chemistry has been developed

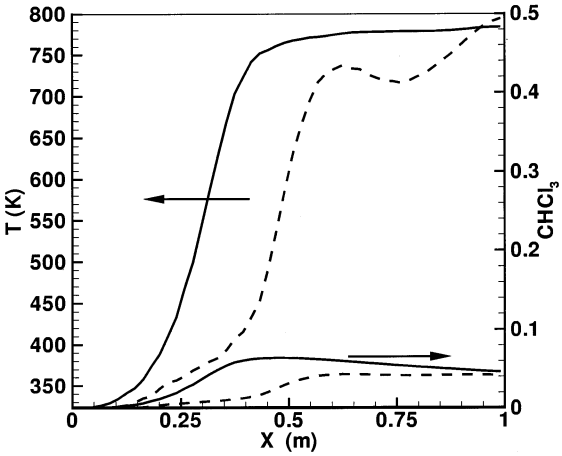

Figure 11. Centerline temperature and product profile using (solid) infinitely fast micromixing condition and (dashed) IEM mixing model for nonpremixed inlets with chlorine in the outer stream.

and used to simulate a gas-phase chlorination reactor. A coaxial jet-stirred reactor has been analyzed for different inlet feed-stream configurations. The detailed chemistry mechanism used enabled the study of the reactor in terms of free-radical formation and transport. The use of ISAT made the computations tractable on a single processor.

The premixed case offers the best performance, with a high chloroform yield and maximum reactor stability. In the case of segregated inlets, it is safer to use chlorine as the inner stream. This prevents a high mass fraction of chlorine or chlorine free radicals in the recirculation zone. Although reactor performance in terms of product yield is only slightly lower than in the premixed case, the reactor operation itself is unstable and is prone to extinction. Accurate inlet control needs to be exercised to keep the reactor lit. Also, with such high temperatures, the formation of carbon soot is more probable and can lead to the deposition of particles on the reactor surface. This will limit the industrial throughput of the coaxial reactor. The last case that was studied used chlorine in the outer stream. This conceivably led to high temperatures, with much of the enthalpy trapped in the recirculation zone. The dynamics of the reactor are inherently unstable, with a high probability of reactor runaway. The reactor stability is determined only by the fraction of organic stream that can get inside the recirculation zone. Higher mass fractions will eventually lead to complete hydrocarbon decomposition and formation of soot particles. Hence, the interaction of jet mixing and reaction is important in predicting the reactor performance.

The scatter plots showed that the reaction equilibrium is attained at very high temperatures for high chlorine fractions. They also showed that the chloroform yield can be as high as 28% by mass, whereas even the premixed case can produce only 14%. The reaction branch also showed that it is detrimental to have a high chlorine or organic mass fraction as this might lead to product decomposition at high temperatures. The conditioning on the mixture fraction reduces the dimensionality of the problem. However, simple hydrodynamic models can be used to study the equilibrium surface for different inlet feed compositions. It was also seen that, in the nonpremixed case with chlorine as the inner stream, the reactor stays lit, and the particles near the outlet lie on the reaction branch. However, in the case with chlorine as the outer jet, the particles near the outer jet collapse onto the mixing branch, showing global extinction. However, particles near the reacting zone were found to produce higher mass fractions of chloroform. Longer residence times in the high-temperature recirculating flow eventually led to product decomposition.

It was found that closure at the subgrid level for the scalars changes the structure and location of the reaction zone. For nonpremixed inlets, the use of completely micromixed conditions leads to higher temperatures and lower product yields than in those cases with a subgrid-level micromixing model. However, for the premixed case, faster mixing widens the jet core and dilutes the recirculation region. This leads to lower temperatures and a decrease in the chlorine consumption. Further study is required that might involve other micromixing closures to determine the effect of the choice of the model on reaction. The present study provides an understanding of the fundamental dynamics of the reactor. It is seen that the recirculation zone helps to sustain the reactor by enthalpy feedback. The different feed-stream configurations change only the location of the reaction zone. The stability is still provided by limited heat recirculation back to the cold inlet stream to preheat the reactants until ignition. It is also seen that, when the enthalpy is trapped in a limited reaction zone (as in the case with chlorine in the outer jet), global extinction might occur even though hot spots are present near the inlet zone.

The reactor configuration can be analyzed for scale-up using the method illustrated in this paper. Because both the flow and the reactions are fully considered, dependence on flow characteristics such as the reattachment length can be studied with detailed chemistry. The inlet jet velocity can be used to control the strength of the recirculation zone and also the effective residence time in the reactor. The effect of unequal momentum and velocity ratios of the jet on mixing and reaction should also be studied.

Acknowledgment

The authors thank the U.S. National Science Foundation (CTS-9720205 and CTS-9996242) and the Dow Chemical Company for support for this project. The authors also thank Prof. Stephen B. Pope for providing the ISAT software used in the simulations.

Literature Cited

(1) Tirtowidjo, M. Presented at the AIChE Annual Meeting, Los Angeles, CA, Nov 16−21, 1997.

(2) Shah, J. J.; Fox, R. O. *Ind. Eng. Chem. Res.* **1999**, *38* (11), 4200−4212.

(3) West, D. H.; Hebert, L. A.; Pividal, K. A. Presented at the Fall AIChE Annual Meeting, Dallas, TX, Oct 31−Nov 5, 1999.

(4) Liu, C.; Barkelew, C. H. *AIChE J.* **1985**, *32*, 1813.

(5) Acharya, S.; Jang, D. S.; West, D. H.; Hebert, L. A. Presented at the AIChE Spring National Meeting, Houston, TX, Apr 7−11, 1991.

(6) Oran, E. S.; Boris, J. P. *Numerical Simulation of Reactive Flow*, 2nd ed.; Cambridge University Press: New York, 2001.

(7) Xu, J.; Pope, S. B. *Combust. Flame* **2000**, *123*, 281−307.

(8) Jones, W. P.; Khaki, M. *Combust. Flame* **1998**, *115* (210−229).

(9) Raju, M. S. *Numer. Heat Transfer A* **1996**, *30*, 753−777.

(10) Tsai, K.; Fox, R. O. *AIChE J.* **1996**, *42*, 2926.

(11) Raman, V.; Fox, R. O.; Harvey, A. D.; West, D. H. *Ind. Eng. Chem. Res.* **2001**, *40*, 5170−5176.

(12) Raman, V.; Fox, R. O.; Harvey, A. D., manuscript to be submitted.
(13) Ferziger, J. H.; Peric, M. *Computational Methods for Fluid Dynamics*, 3rd ed.; Springer: New York, 2002.
(14) Pope, S. B. *Combust. Sci. Technol.* **1981**, *25*, 159−174.
(15) Haworth, D. C.; Tahry, S. H. E. *AIAA J.* **1991**, *29* (2), 208−218.
(16) Muradoglu, M.; Jenny, P.; Pope, S. B.; Caughey, D. A. *J. Comput. Phys.* **1999**, *154*, 342−371.
(17) Xu, J.; Pope, S. B. *J. Comput. Phys.* **1999**, *152*, 192−230.
(18) Shuen, J. S.; Chen, K. H.; Choi, Y. *J. Comput. Phys.* **1993**, *106*, 306−318.
(19) Edwards, J. R. *Comput. Fluids* **1997**, *26*, 645−659.
(20) Rodi, W.; Mansour, N. N. *J. Fluid Mech.* **1993**, *250*, 509−529.
(21) Pope, S. B. *Combust. Theory Model.* **1997**, *1*, 41.
(22) Subramaniam, S.; Haworth, D. *Int. J. Eng. Res.* **2000**, *1*, 171−190.
(23) Jones, W. P.; Launder, B. E. *Int. J. Heat Mass Transfer* **1972**, *15*, 301.
(24) Pope, S. B. *Prog. Energy Combust. Sci.* **1985**, *11*, 119.
(25) Pope, S. B. *Combust. Flame* **1976**, *27*, 299−312.
(26) Roekaerts, D. *Appl. Sci. Res.* **1991**, *48*, 271.
(27) Jenny, P.; Pope, S. B.; Muradoglu, M.; Caughey, D. A. *J. Comput. Phys.* **2001**, *166*, 218−252.
(28) Mobus, H.; Gerlinger, P.; Bruggemann, D. *Combust. Flame* **2001**, *124*, 519−534.
(29) Maas, U. A.; Pope, S. B. *Combust. Flame* **1992**, *88*, 239.
(30) Villermaux, J.; Falk, L. *Chem. Eng. Sci.* **1994**, *49* (24B), 5127−5140.
(31) Valino, L.; Dopazo, C. *Phys. Fluids A* **1991**, *3*, 3034.
(32) Subramaniam, S.; Pope, S. B. *Combust. Flame* **1999**, *117*, 732.

Received for review August 21, 2002
Revised manuscript received October 24, 2002
Accepted October 28, 2002

IE0206599